31st Annual International Conference of the IEEE EMBS
Minneapolis, Minnesota, USA, September 2-6, 2009

Photoacoustic Imaging Endoscope

C. Sheaff, N. Lau, H. Patel, S.-W. Huang, *Member, IEEE*, and S. Ashkenazi, *Member, IEEE*

***Abstract*—We currently present a design concept for a photoacoustic imaging endoscope as well as some preliminary experimental results. The device is based on the generation of acoustic waves in tissue by short laser pulses and the sensing of these waves with a thin, optical Fabry-Pérot etalon. The entire device is designed to be mounted on the tip of a needle to deliver high-resolution photoacoustic imaging for minimally-invasive clinical applications such as diagnosing kidney disease and guiding laparoscopic surgery.**

I. Introduction

The number of studies involving photoacoustic imaging for medical applications has rapidly increased during the last decade (see [1] for a comprehensive review). The basic principle is both simple and appealing. A short pulse of laser light illuminates a tissue, creating an almost instantly small increase in temperature in parts of the tissue that absorb the light. These parts then undergo thermal expansion and launch an acoustic wave characterized by a very wide bandwidth (limited primarily by the duration of the laser pulse). The generated waves propagate and are then detected by an ultrasound imaging array. High resolution images of the acoustic sources (optical absorbers) can be formed using the data received by the array and ultrasound reconstruction algorithms. The unique advantages of photoacoustic imaging stem from the combination of the high contrast and specificity of optical imaging with the high resolution of ultrasound imaging. These benefits have been clearly demonstrated in a range of medical applications such as breast cancer diagnosis [2], lymph node visualization [3], functional brain imaging [4], and skin burn imaging [5].

One of the major limitations of this technique is its depth of penetration, limited by both optical and acoustical attenuation. Optical penetration depth depends on the choice of wavelength. In the visible range - typically green light (532 nm) - doubled Nd:YAG lasers are used giving in an imaging depth of up to 3 mm. Deeper penetration is achieved using near-infrared sources. In the range of 700 nm to 1064 nm, imaging depth of up to 2 cm has been demonstrated. Acoustic attenuation is much smaller than optical attenuation in most cases and thus does not further limit imaging depth. However, at frequencies higher than 50 MHz, acoustic attenuation should also be considered.

In this work we describe our approach for minimally-invasive, high-resolution photoacoustic imaging of deep underlying tissue well beyond the reach of optical penetration. Our prime motivation is to develop a tool for diagnosing kidney disease and image-guided biopsy. The device design is based on an optoacoustic thin-film imaging sensor mounted on the tip of a needle. In the following, we will describe our design concept for a needle-based photoacoustic imaging system for minimally-invasive applications.

II. Etalon detector

A. General

Optical detection of ultrasound has been studied for several decades, mostly as a method of non-contact ultrasonic sensing or visualization [6]. During recent years focus has shifted to utilizing micro-optics for miniaturization of ultrasound detection [7, 8]. Although conventional piezoelectric detectors provide better sensitivity for most applications, optical techniques outperform them in cases where small detectors (<100 μm) are required. Moreover, optical detection and laser-generated ultrasound for photoacoustic imaging can be conveniently integrated into a single imaging device. Here we describe a specific implementation of optical detection of ultrasound using a thin-film etalon as an imaging sensor array.

B. Principles of operation

A thin-film etalon is a Fabry-Pérot interferometer made of a transparent film sandwiched between two coated mirror layers. Multiple optical reflections between the mirrors are established thereby leading to a sharp resonance curve. Due to this sharpness, reflection of an optical beam at a wavelength near resonance is highly sensitive to small variations in the thickness of the cavity. Ultrasound waves happen to alter the etalon thickness by inducing small displacements of one or both of the mirror layers. Therefore acoustic waves can be detected by measuring the variations in intensity of a laser beam reflected off the surface of the etalon.

C. Structure

Fabrication of an etalon sensor involves gold (or dielectric) mirror deposition by vacuum e-beam evaporation onto a glass substrate, polymer spin-coating of a spacer layer, and a second mirror deposition similar to the first. The

Manuscript received April 7, 2009. This work is supported by the University of Minnesota, Center for Medical Devices, and in part by the NIH National Institute of Biomedical Imaging and BioEngineering (NIBIB) grant EB003455.

C. Sheaff, N. Lau, H. Patel, and S. Ashkenazi are with the Department of Biomedical Engineering, University of Minnesota, Minneapolis, MN 55455 USA (corresponding author: Shai Ashkenazi, email: ashke003@umn.edu, phone: 612-625-6107).

S.-W. Wang is with the Department of Bioengineering, University of Washington, Seattle, WA 98195.

spacer layer is made of SU-8 polymer film (Microchem) in the range of 6 to 10 µm. The structure of the etalon is shown in Figure 1.

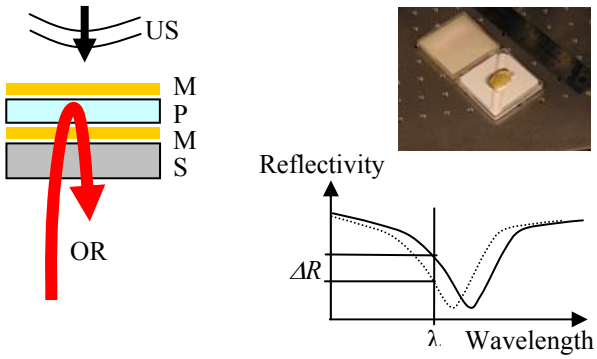

Fig. 1. The Etalon ultrasound detector is composed of a thin transparent polymer layer (P) sandwiched between two mirrors (M) on top of a glass substrate (S). Ultrasound waves (US) cause a change (ΔR) in the optical reflectivity (OR) at wavelength (λ) near resonance. (upper right) Photo of the etalon detector.

D. Sensitivity

The sensitivity of the etalon depends on its thickness, the probing beam power, and the resonance sharpness (quality factor). It is measured and specified as a noise-equivalent pressure (NEP) - the level of acoustic pressure required to produce a signal equal in magnitude to the root-mean-square of the noise level. Without any further signal averaging, NEP is the minimum acoustic pressure that can be detected by the etalon. We have measured an NEP of 6.5 kPa (at a signal bandwidth of 40 MHz) for a 6 µm SU-8 etalon, illuminated by a 180 µW beam.

E. Bandwidth

The bandwidth of a 6-µm SU-8 etalon was measured by detecting its response to a short acoustic impulse generated by pulsed laser (5 ns period) absorption on a thin layer of Chromium coated on a glass plate, placed 0.5 mm above the etalon. The etalon signal is shown in Figure 2 along with the temporal profile of the laser pulse detected with a silicon PIN diode. Spectral analysis of the signals shows a detection bandwidth of 80 MHz.

F. Array operation

Imaging relies on ultrasound detection at multiple locations, typically via a 1-D or 2-D array. Two schemes are available for multipoint probing of the etalon. In the first, a focused beam illuminates a small spot on the etalon's surface and the reflected beam is collected by a photo-detector. Acoustic wave detection at multiple locations is achieved by scanning the optical spot. A second method utilizes wide, collimated-beam illumination of the etalon's surface and focusing optics (lens) to collect the reflected beam from an array of tight spots on the etalon with an array of photo-detectors, thus providing parallel detection at multiple points. The first method has a higher signal-to-noise-ratio (SNR) due to higher optical fluence at the active area, whereas the second method is preferred for faster data acquisition. The choice between the two methods depends on application requirements such as dynamic range and image frame rate. An intermediate method can also be used, where a number of focused beams are scanned across the etalon and the reflected beams are collected by an array of photo-detectors.

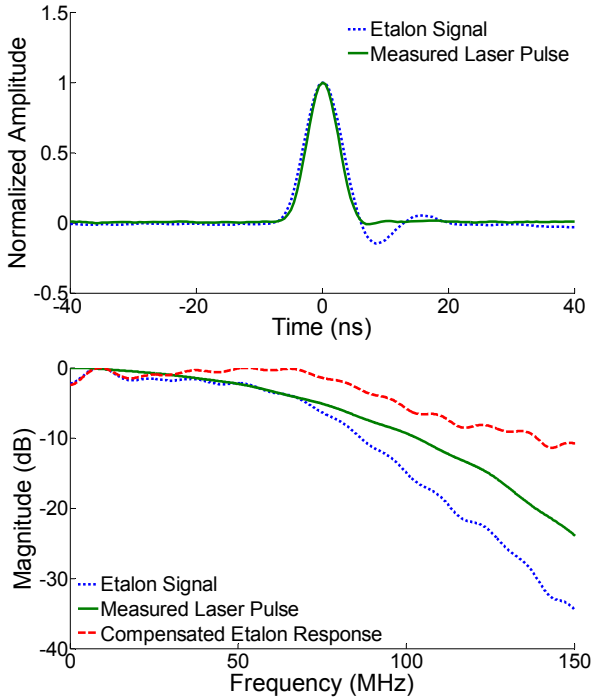

Fig. 2. (top) Etalon signal (dotted line) in response to a broadband acoustic wave generated by short laser pulse (solid line) absorption on a thin Chromium film deposited on a glass substrate. (bottom) Frequency domain representation of the Etalon signal (dotted line), laser pulse (solid line), and Etalon frequency response (dashed line).

III. INTEGRATED DEVICE DESIGN

We have designed a photoacoustic-imaging endoscope for minimally-invasive medical imaging. A 1mm endoscope housed in a gauge-17 needle (1.5 mm OD) is used for light delivery to a front end etalon device mounted on the tip of the needle. A schematic of the proposed device is given in Figure 3. A CW tunable laser (4mW, 1520 – 1620 nm) is used to probe the etalon. The laser output is delivered by an optical fiber to a circulator and then to a fast optical scanner of the laser-focused spot across the back surface of a graduated refraction index (GRIN) lens. The GRIN lens maps the optical field from the back plane to its front end surface where the etalon is mounted. This system provides a stable and fast scanning of the focused beam on the etalon surface. The reflected intensity is delivered back through the GRIN lens and the scanning optics to the circulator where it is routed from the output port to a photodetector.

A pulsed laser emitting at 532 nm is used for exciting photoacoustic waves in tissue. The pulsed illumination is delivered through the optical scanner and the GRIN lens

system. The excitation pulsed laser beam is transmitted to the tissue through the etalon by using wavelength-selective mirrors.

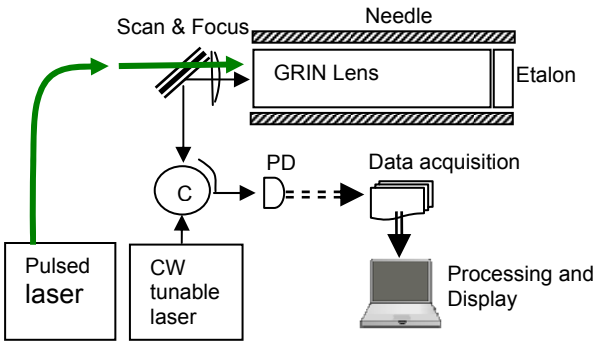

Fig. 3. Device schematic: A pulsed laser beam is delivered by fiber optics to a GRIN lens mounted inside a needle. A CW beam is focused and scanned on the back side of the GRIN lens. The focal plane is mapped to the etalon surface that is mounted on the front face of the lens. The reflected beam is routed through a circulator and captured by a photodetector. High-speed digitizers and a desktop computer are then used for data acquisition and processing thereby rendering a photoacoustic image.

IV. PHOTOACOUSTIC IMAGING

We have performed preliminary experiments to test the resolution as well as other parameters of photoacoustic imaging using a 6 µm thick etalon sensor. The experimental system was designed to work in a parallel detection mode. A 1.3 mm wide (-3 dB) collimated beam of a tunable laser (HP 8168F, 5mW) was used to illuminate the etalon. The reflection from a 50 µm size spot on the etalon was collected with a lens and then captured by a photodetector (1811-FC, New Focus, San Jose, CA). Mechanical scanning of the photodetector was used to acquire optical reflections from a square array of points on the etalon surface (23 x 23 points, at 50µm spacing). The illumination power at each array location was 1.8 µW. Signals from the photodetector were first amplified by 30dB and then digitized by an oscilloscope (Lecroy WaveSurfer 432). A group of three black polystyrene beads of 50 µm in diameter were embedded in a gel and used as a phantom target for photoacoustic imaging. The phantom was illuminated by a doubled Nd:YAG pulsed laser emitting at 532 nm (Surelite I-20, Continuum, Santa Clara, CA), and the pulse energy density was 28 mJ/cm^2.

Shown in Figure 4c is a photoacoustic image of one of the beads of the phantom, obtained by coherent summation of the signals from the full 23 x 23 etalon array. In order to minimize scan time, minimizing the number of elements in use is essential. We therefore seek the fewest number of elements that will yield an image quality comparable to that which makes use of all elements. Figure 4b demonstrates the quality of the bead image that was constructed using only 50% percent (randomly selected) of the original 23 x 23 elements. In comparison, it can be seen that the image background noise increases by using only half of the array elements. This can be attributed to reduced suppression of side lobes causing interference signals from other beads in the phantom, and also to higher electronic noise due to 50% reduction in signal averaging. As shown in Figure 4a, the 3-D field calculated using a range of percentages of the original elements was correlated with that produced using all elements. 10 realizations using randomly-generated, sparse arrays were averaged at each percentage to eliminate any spatial dependence. As expected, the correlation coefficient approaches a value of one as the number of elements used increases. The plotted results suggest that using only approximately 60% of the 23 x 23 array can achieve an image of 95% accuracy with respect to the original.

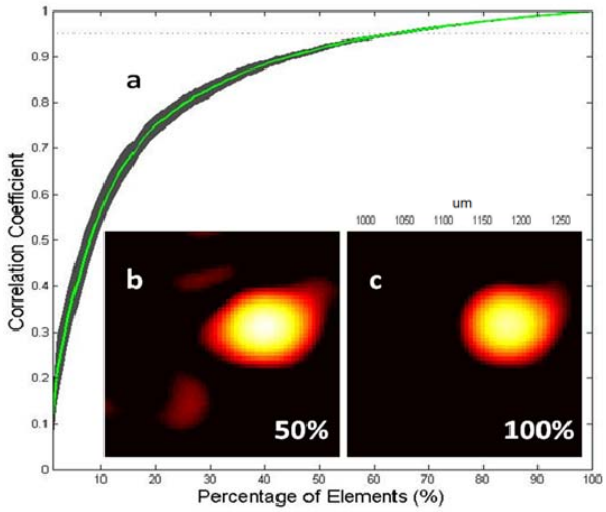

Fig. 4. (a) Correlation of photoacoustic image reconstructed using random sparse array with corresponding image using the full 23 x 23 elements array. (b) Photoacoustic image of a 50 µm size black polystyrene bead reconstructed using 50% of the full array elements. (c) Same image reconstructed using the full array

V. CONCLUSION

We have presented here a device design for an endoscopic imager based on photoacoustic generation and etalon detection of ultrasound. Photoacoustic signal generation provides high contrast for blood vasculature imaging and etalon detection is optimal for high density array of small element size. Etalon characterization shows better sensitivity and wider bandwidth than similar size piezoelectric transducers. Following the refinement and optimization of the device characteristics, the applications of image-guided biopsy and tissue analysis of the kidney will be explored. If successful, this work could lead to a new minimally-invasive technique for analyzing diseased tissue in a number of applications which may not only provide new information about disease progression but may also improve biopsy procedures by enhancing the precision of tissue extraction.

ACKNOWLEDGMENT

This work is supported by the University of Minnesota, Center for Medical Devices, and in part by the NIH National

Institute of Biomedical Imaging and BioEngineering (NIBIB) grant EB003455.

REFERENCES

[1] L. V. Wang, Photoacoustic Imaging and Spectroscopy (Optical Science and Engineering), CRC Press, 2009.

[2] A. A. Oraevsky, A. A. Karabutov, S. V. Solomatin, E. V. Saveteeva, V. G. Andreev, Z. Gatalica, H. Singh, and R. D. Fleming; Laser optoacoustic imaging of breast cancer in vivo; *SPIE Proc.* **4256**, p.6 (2001).

[3] K. H. Song, E. W. Stein, J. A. Margenthaler, and L. V. Wang; Noninvasive photoacoustic identification of sentinel lymph nodes containing methylene blue in vivo in a rat model; *J. Biomed. Opt*. **13**, 054033 (2008).

[4] X. Wang, G. Ku, X. Xie, Y. Wang, G. Stoica, and L. V. Wang, "Noninvasive functional photoacoustic tomography of blood-oxygen saturation in the brain", *Proc. SPIE*, **5320**, p.69 (2004).

[5] M. Yamazaki, S. Sato, H. Ashida, D. Saito, Y. Okada, and M. Obara, "Measurement of burn depths in rats using multiwavelength photoacoustic depth profiling", *J. Biomed. Opt*, **10**, p. 64011, (2005).

[6] R. Czarnek, C. -J. Yu, F. R. Dax, "High efficiency interferometer for non-contact detection of ultrasounds", *Proc. SPIE*, **2544**, p 210, 1995.

[7] Y. Hou, J. S. Kim, S. –W. Huang, S. Ashkenazi, L.J. Guo, and M. O'Donnell; "Characterization of a broadband all-optical ultrasound transducer-from optical and acoustical properties to imaging" IEEE Trans. Ultrason. Ferroelect. Freq. Contr. 55, (8), p.1867 – 1877 (2008).

[8] S. Ashkenazi, C. Y. Chao, L. J. Guo, and M. O'Donnell, "Ultrasound detection using polymer microring optical resonator", Appl. Phys. Lett. 85, pp. 5418-20 (2004).